11 Jul 2022

A Comparative Study on Representativeness and Stochastic Efficacy of Miniature Tensile Specimen Testing

Sreekar Karnati

Sriram Praneeth Isanaka
Missouri University of Science and Technology, sihyd@mst.edu

Yunlu Zhang

Frank W. Liou
Missouri University of Science and Technology, liou@mst.edu

et. al. For a complete list of authors, see https://scholarsmine.mst.edu/mec_aereng_facwork/4935

Recommended Citation

S. Karnati et al., "A Comparative Study on Representativeness and Stochastic Efficacy of Miniature Tensile Specimen Testing," *Materials Performance and Characterization*, vol. 11, no. 3, ASTM International, Jul 2022.
The definitive version is available at https://doi.org/10.1520/MPC20210136

Materials Performance and Characterization

doi:10.1520/MPC20210136 / Vol. 11 / No. 3 / 2022 / available online at www.astm.org

Sreekar Karnati,[1] Sriram Praneeth Isanaka,[2] Yunlu Zhang,[2] Frank F. Liou,[2] and Jason L. Schulthess[3]

A Comparative Study on Representativeness and Stochastic Efficacy of Miniature Tensile Specimen Testing

Reference

S. Karnati, S. P. Isanaka, Y. Zhang, F. F. Liou, and J. L. Schulthess, "A Comparative Study on Representativeness and Stochastic Efficacy of Miniature Tensile Specimen Testing," *Materials Performance and Characterization* 11, no. 3 (2022): 424–439. https://doi.org/10.1520/MPC20210136

ABSTRACT

In this article, a miniature dog bone tensile coupon design was tested against the existing ASTM standard specimen design. Specimens were prepared from commercially sourced austenitic stainless steel 304 alloy, and a defect-ridden additively manufactured 304L alloy was studied. By utilizing a tensile specimen design that is 1/230th volume of the smallest ASTM E8-04 (2016), *Standard Test Methods for Tension Testing of Metallic Materials*, dog bone specimen, coupled to a digital image correlation (DIC) setup, case studies were performed to compare tensile property measurements and strain field evolution. Whereas yield strength measurements were observed to be similar, post-yield, the ultimate strength measurements and ductility measurements from the miniature specimens were observed to be higher than the ASTM specimen design. Although the strength measurements were comparable, the strain evolution was found to differ in the miniature specimens. Studies to assess effects of varying thickness and defect population were also pursued on the miniature tensile specimen. From the DIC strain field estimations, the peak local strain values at ultimate tensile strength were observed to be increasing with reducing specimen thickness. Testing of defect ridden stainless steel revealed the sensitivity to failure through strain localization and the influence of defect size was captured in the strength measurements.

Keywords

miniature tensile testing, digital image correlation, stochastic modeling, high throughput testing, benchmarking study

Manuscript received December 21, 2021; accepted for publication April 26, 2022; published online July 11, 2022. Issue published October 11, 2022.

[1] Department of Mechanical and Aerospace Engineering, Missouri University of Science and Technology, 400 W 13th St., Rolla, MO 65409, USA (Corresponding author), e-mail: skw92@mst.edu, https://orcid.org/0000-0002-6358-0693

[2] Department of Mechanical and Aerospace Engineering, Missouri University of Science and Technology, 400 W 13th St., Rolla, MO 65409, USA

[3] Idaho National Laboratory, 1955 N Fremont Ave., Idaho Falls, ID 83415, USA, https://orcid.org/0000-0002-4289-7528

Introduction

Knowledge of material performance and stability is critical for assessing and identifying candidate materials for various applications. Such knowledge is necessary to design components that can perform reliably through their intended lifespan. Various attributes and parameters of material performance are gathered by performing extensive mechanical characterization. Currently, there exist standard methods to perform these characterization studies for various mechanical properties.[1] However, in the current day, the drive for efficiency and compactness has driven designers and manufacturers toward fabricating components with smaller footprints and feature definitions. Often, the volume of critical sections of these components is much smaller than the volume of specimens used for mechanical characterization. This raises the issue of the relevancy of characteristic data gathered through existing standard specimen designs.[2] Although lowering the gauge volume appears to be an obvious solution, the representativeness of these small test volumes still has to be investigated in detail.[3,4] Beyond relevance, the use of miniature specimens also improves the economy and efficiency of characterization processes. The use of miniature specimens is particularly beneficial to the nuclear industry or other sectors where the materials employed are either expensive to manufacture or dangerous to handle. Extensive characterization is warranted for material design and discovery, and the study of designs for nuclear components also requires exposure of test material to radiation.[5] The larger specimen volume required by existing standards requires relatively vast amounts of material leading to a slow and expensive characterization process. These large specimen-based tests also lead to more radioactive waste creating concerns during disposal.

Data vital to designers from all industries, such as ultimate tensile strength (UTS), yield strength, ductility, and strain hardening exponent can be measured using tensile testing. Developing a viable and valid miniature tensile (MT) testing methodology would be not only relevant but also immensely valuable.[6] In the past, the influence of microstructural features such as grain size, grain shape, phase composition, and their dimensions in comparison to the miniaturized tensile coupon has been well studied.[7] Threshold criteria such as a minimum of 20 grains across the gauge section, and gauge thickness to average grain size ratio of at least 6–10 has been well established,[8,9] and meeting these threshold requirements ensures representative and repeatable measurement of mechanical properties. However, these measurements can also be influenced by the geometry of the tensile coupon. Particularly, the ductility measurements can vary with specimen designs. The correlation of mechanical properties obtained from different specimen geometries has been studied and reported by many researchers. Variation in strength measurements with gauge length in titanium alloys,[3] increasing and stabilizing strength and ductility measurements with increasing thickness to width aspect ratio in stainless steel 316,[10] and variation with ductility measurements with gauge length to thickness ratio have been reported.[11] Although efforts have been pursued to understand the variation of measurements from miniature specimens with varying geometry, benchmarking efforts comparing these measurements to those obtained from standard bulk specimen designs still need to be pursued. In the current effort, a benchmarking study comparing the measurements obtained from a MT coupon design is compared against those measured using an ASTM standard specimen design. In addition to comparing the bulk measurements, digital image correlation (DIC) methodology was also employed to estimate strain field evolution and compare the same between the two specimen designs.

The economic advantages from testing of MT specimens provide the feasibility to perform large-scale stochastic performance modeling.[12] Insights from such modeling will be crucial in forecasting failure in designed components. Therefore, the sensitivity of such analyses to varying specimen thickness is a topic of great interest. Confidence in the ability to amass stochastic information from small volumes of material will be valuable for alloy development, process development, and lifetime assessment applications.[7] In the current effort, variation of the stochastic distribution of mechanical properties with material thickness is presented to demonstrate the efficacy of the stochastic data acquired through the miniature specimen design.

The advantages of the small-gauge volume are not just limited to the economy of the testing process. The small volume of the gauge section increases the sensitivity of the testing methodology by decreasing the critical defect size, which is exhibited by many modern processes like additive manufacturing (AM) and novel materials like

functionally graded materials (FGMs). This increased sensitivity will be effective in realizing inhomogeneity within materials.[13] It will be a valuable tool from a quality perspective as well, where batch to batch, within batch, vendor to vendor, etc. variations in the stock material can be accurately evaluated.[12] The small gauge volume can also be effective in establishing spatial maps of material performance within a single material stock.[14] Miniature specimen characterization can serve as a robust tool for the qualification of a process in the manufacturing industry. To evaluate this capability, porosity-ridden material produced through AM was tested and presented. Strain field evolution captured through the DIC technique was used to capture strain localization and failure initiation.

Materials and Methods

MATERIALS

Commercially sourced cold-rolled and annealed stainless steel AISI 304 alloy material with traceable lot and material certificate information was used for the benchmarking and stochastic sensitivity studies. The grain size for this material was no. 4 as per the ASTM E112-13(2021), *Standard Test Methods for Determining Average Grain Size*, grain size measurement standard. This size was deemed sufficient to meet the minimum grain size threshold for MT specimens. Additive manufactured AISI 304L was used for sensitivity identification and characterization. The additively manufactured material studied in the current investigation was fabricated using the Renishaw AM 250 located at Missouri University of Science and Technology. The AM 250 is equipped with an Nd-YAG pulsed laser capable of producing a peak power of 200-W beam with a Gaussian intensity profile. During the deposition, the substrate and powder in the chamber were maintained at 80°C to reduce the influence of water content in the powder. A constant volumetric recirculating gas flow of 400 ft/mm^3 argon gas was maintained to remove melt ejecta and condensate generated during laser powder bed fusion (L-PBF). Process parameters of the AM250 machine were adjusted to create a bulk relative density of 97 % in the additively manufactured AISI 304L material, which was validated through Archimedes' principle-based density testing. For metallographic evaluation representative volume sections were cut and examined. These sections were mounted in epoxy, ground with abrasive articles (400, 600, 800, and 1,200 grit) and polished with silica suspension (9, 3, 1, and 0.05 μm). Electro-etching was performed in 40-ml deionized water and 60-ml HNO_3 mixture at a voltage of 5 V for 5 s. The microstructure of the specimens was examined and imaged under an optical microscope (OM, Hirox KH-8700 microscope).

EXPERIMENTAL SETUP

Two specimen designs were tested under this effort. The subsize dog bone specimen design from the ASTM E8-04 (2016), *Standard Test Methods for Tension Testing of Metallic Materials*, standard was chosen as the macrosize specimen. Missouri S&T developed MT design that was used as the mini/mesoscale specimen. The MT specimen is 1/230th in volume compared to the ASTM specimen. The drawings of these specimens and representative examples after testing are shown in **figure 1**. The ASTM specimens were machined to standard specifications. The MT specimens were machined using a wire-electric discharge machine; additional details are discussed below.

The final surface finish and recast layer formation were two key attributes that needed close examination and optimization during the development of MT specimen manufacturing process. EDM machining and the relationship between process parameters and surface finish have been well established in the manufacturing and quality control industries.[15] More specifically, the relationship between increasing voltage and current and the increase in material removal rate (MRR)[16] was utilized by this research team in developing a cut plan for the MT specimen design discussed in this article. One rough cutting pass and three finish cutting passes were developed using 0.3-mm-diameter bronze wire to cut miniature specimen that use progressively decreasing MRR through lower voltage and amperage values to target improved specimen dimensionality as shown through the measurements of voltage and amperage of SS304L (**Table 1**).

Although this cut strategy enables the creation of MT specimen with dimensional accuracy along the profile (measured length and width values in **Table 2**), the top and bottom surfaces of the specimen still warrant finish

FIG. 1 (*A*) Illustrations of the ASTM E8-04 dog bone specimen; (*B*) miniature tensile (MT) specimen; all dimensions are in millimeters, and drawings are not to scale; (*C*) comparison between the two specimen designs.

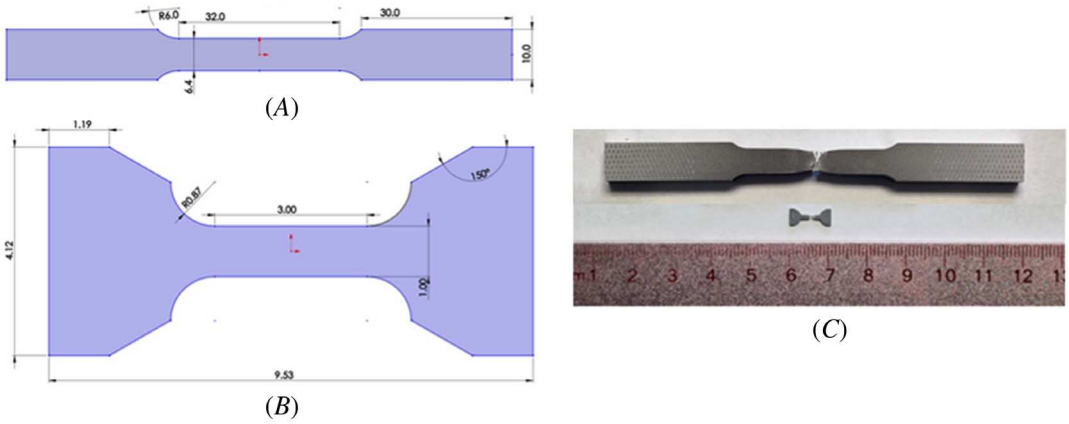

TABLE 1
EDM cut plan and average voltage and amperage values for MT specimen

Cut Pass	Manufacturing Rationale	Voltage (V)	Amperage (I)
1	Roughing	34	1.9
2	First finishing	67	0.6
3	Second finishing	57	0.9
4	Third finishing	15	0.5

TABLE 2
Details and mechanical property measurements obtained from different specimen designs

		Conventional			DIC		
Variable	Specimen Type	# Tested	Mean	Standard Deviation	# Tested	Mean	Standard Deviation
0.2 % Offset yield strength, MPa	ASTM	7	256.4	9.5	3	250.0	8.6
	MT-0.5 mm	38	275.2	24.8	3	269.5	1.5
	MT-0.75 mm	37	280.4	17.1	4	265.3	3.6
	MT-1 mm	39	268.6	15.0	4	253.3	3.1
Ultimate tensile strength, MPa	ASTM	7	667.2	5.6	3	665.7	4.9
	MT-0.5 mm	39	728.1	9.8	3	731.0	1.0
	MT-0.75 mm	37	730.8	8.8	4	727.8	3.3
	MT-1 mm	39	736.9	8.1	4	731.1	3.8
Strain at break, mm/mm	ASTM	7	0.84	0.03			
	MT-0.5 mm	39	1.09	0.02			
	MT-0.75 mm	37	1.13	0.03			
	MT-1 mm	39	1.17	0.02			

machining to remove the oxide layer formed as part of EDM. Because of the small form factor of the specimen and nonmagnetic nature of many materials, designing a fixture to automate this stage proves difficult. Therefore, a hand-polishing work plan was developed to remove the oxide layer from EDM while still maintaining the dimensional tolerance of miniature specimen. Example of the procedure developed to remove the oxide layer, measured dimensions before and after hand polishing are shown in figure 2. As can be observed from the images in

FIG. 2 SS304L miniature specimen after EDM. Before 600 and 800 grit polishing (on left) and after polishing (on right).

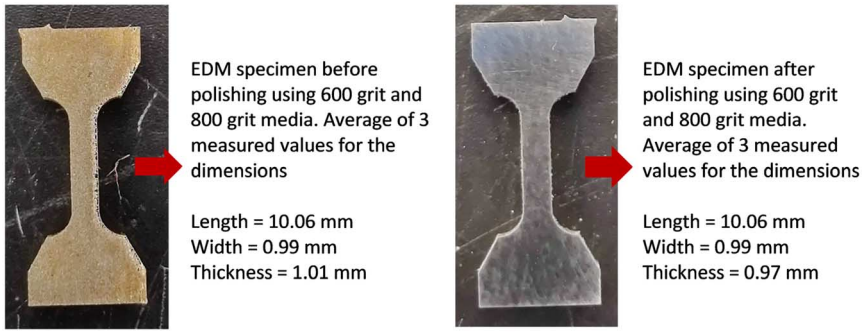

figure 2, the manual polishing work plan developed removes the oxide layer and any burr left behind on the gauge section because of EDM, without aggressively removing material. To maintain consistency and avoid loss of geometry definition, a tolerance of 0.05 mm is followed for the width and thickness of the gauge length.

The MT testing setup at Missouri S&T was developed to be a testbed for the design and setup of DIC coupled tensile testing. Choosing the right lens and camera combination is key to ensuring that the depth of focus of the DIC apparatus spans the potential out-of-plane motion of the specimen across the different specimen sizes and grip shapes. The main differentiators among the hardware setups are the type of lens used and the size of the camera's sensor. The types of lenses used were a macrolens for monitoring ASTM (Laowa 60-mm f/2.8 2X Ultra-Macro, Anhui, China) specimens and telecentric lens (RT-HR-1M71; Opto Engineering, Houston, TX, USA) for monitoring MT specimens. The camera (ASTM setup: BFS-U3-200S6M-C; FLIR Systems; MT setup: BFS-U3-50S5M-C; FLIR Systems, Wilsonville, OR) was controlled through a custom written code developed using the SDK kit provided by the camera manufacturer. The best possible accuracy for the setup was in the case of MT evaluations; a resolution of 0.5 μm was perceived to be achievable. For the DIC analysis, at 20-mega-pixel image resolution and 8-FPS image acquisition speed, the points of interest (POIs)/facets contained 21 by 21 pixels. Along the width of the MT gauge section, approximately 11 POIs were setup.

The setups for the case of E-8 subsize and miniature specimens are shown below in figure 3. Whereas the ASTM specimens were fixtured using wedge grips, custom fabricated shoulder grips with self-aligning capability were used for MT specimens. In addition to the DIC measurement, an extensometer was also used to perform elongation measurement. The extensometer was placed on the ASTM specimen during MT specimen testing. Because of its small size, the extensometer was placed on the shoulder grip. The extensometer-based measurement in the MT specimen may be perceived as indirect and includes the contribution from any elongation in the shoulder grips. However, because of the relative dimensional difference, this elongation contribution is assumed to be negligible. A strain rate of 0.2 mm/mm/min was used for testing these specimens. The fracture surfaces of the broken specimens were examined using the ASPEX-PICA 1020 SEM.

METHODS

Strain and Strain Field Estimation

The engineering strain traditionally measured by an extensometer can be derived from the result of DIC analysis. First, two regions at the ends of the gauge section of the tensile specimen are defined. The POIs inside the two regions are extracted and plotted in figure 4. These POIs serve the same functionality as the physical extensometer and can be treated as a virtual extensometer. The locations of the POIs on the virtual extensometer are tracked at specified time intervals. The POI tracking is pursued through image processing techniques available from the DIC techniques.[17] The engineering strain is then calculated by the equation the locations of the POIs on the virtual extensometer are tracked at specified time intervals. The engineering strain is then calculated by the equation

FIG. 3 DIC hardware incorporated into the Missouri S&T test setup for ASTM E8-04 subsize dog bone specimens (left) and miniature tensile specimens (right).

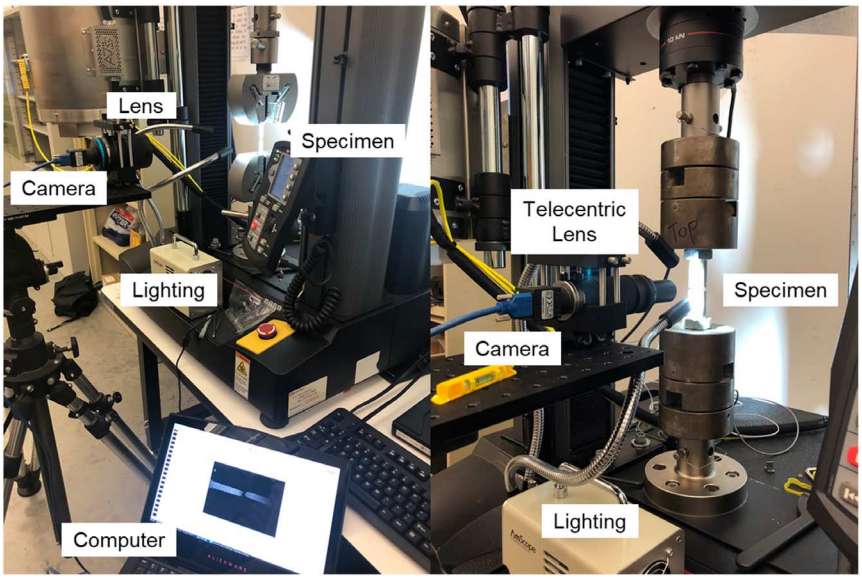

FIG. 4

Points of interest (POIs) of the virtual extensometer.

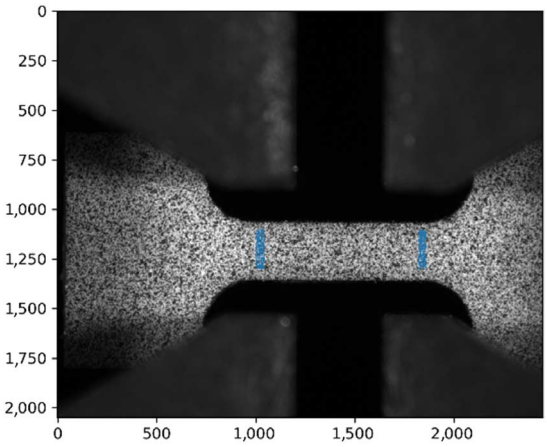

$$e = \frac{\Delta l}{l_0} \tag{1}$$

The engineering strain data is combined with the load data from the tensile machine to derive the engineering stress-strain curve. Engineering stress is calculated from the tensile load and dimensions of the specimen cross section. These two are then used to calculate the engineering stress-strain curve of the specimen as shown in figure 5. Additional properties including yield point, UTS, and fracture strain can also be estimated from this curve. However, it becomes challenging to precisely record the strain at failure due to the video feed being affected by the fracture. The same is captured in the plots shown in figure 5.

FIG. 5 (*A*) The relationship between the measured engineering strain and elapsed time; (*B*) Engineering stress-strain curve generated from combining the DIC data and the stress data; Arrows indicate the erroneous/uncertain estimation since failure.

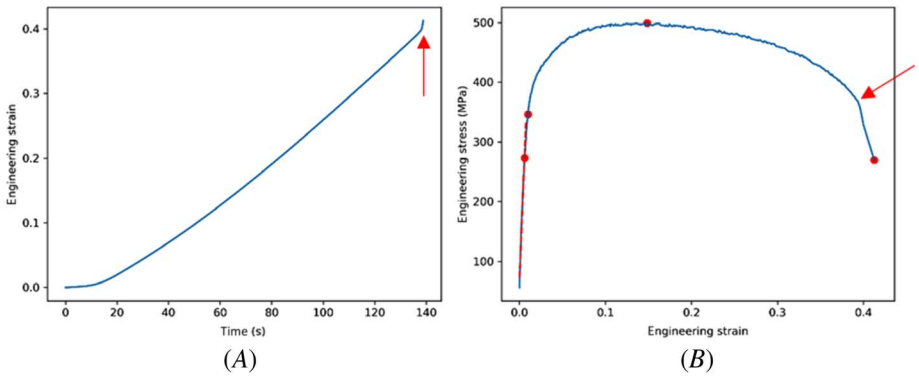

The strain is calculated from the determined displacement field through the equations

$$u(x,y) = u_0 + \frac{\partial u}{\partial x}x + \frac{\partial u}{\partial y}y \tag{2}$$

$$v(x,y) = v_0 + \frac{\partial v}{\partial x}x + \frac{\partial v}{\partial y}y \tag{3}$$

where u, v are the displacements surrounding the POI in the x and y directions respectively, u_0, v_0 are the displacements at the POI in the respective directions, and $\frac{\partial u}{\partial x}, \frac{\partial u}{\partial y}, \frac{\partial v}{\partial x}, \frac{\partial v}{\partial y}$ are the gradients of the displacement field.

In a small region surrounding the POI, the gradients of the displacement field are assumed to be constant. Therefore, they can be solved from the over-constrained system of equations by the least square method

$$\begin{pmatrix} 1 & x_1 - x & y_1 - y \\ 1 & x_2 - x & y_2 - y \\ \vdots & \vdots & \vdots \\ 1 & x_n - x & y_n - y \end{pmatrix} \begin{pmatrix} u_0 \\ \frac{\partial u}{\partial x} \\ \frac{\partial u}{\partial y} \end{pmatrix} = \begin{pmatrix} u_1 \\ u_2 \\ \vdots \\ u_n \end{pmatrix} \tag{4}$$

where n is the number of neighboring POIs used to calculate the local gradient, $x_1, x_2, \cdots, x_n$ and $y_1, y_2, \cdots, y_n$ are the coordinates of these neighboring POIs, and $u_1, u_2, \cdots, u_n$ are the displacements at the neighboring POIs. The equation for the y-direction is similar.

The Green strain is calculated from the gradients

$$\varepsilon_{xx} = \frac{\partial u}{\partial x} + \frac{1}{2}\left(\left(\frac{\partial u}{\partial x}\right)^2 + \left(\frac{\partial v}{\partial x}\right)^2\right) \tag{5}$$

$$\varepsilon_{yy} = \frac{\partial v}{\partial y} + \frac{1}{2}\left(\left(\frac{\partial u}{\partial y}\right)^2 + \left(\frac{\partial v}{\partial y}\right)^2\right) \tag{6}$$

$$\varepsilon_{xy} = \frac{1}{2}\left(\frac{\partial u}{\partial y} + \frac{\partial v}{\partial x} + \frac{\partial u}{\partial x}\frac{\partial u}{\partial y} + \frac{\partial v}{\partial x}\frac{\partial v}{\partial y}\right) \tag{7}$$

The principal strain $\varepsilon_1, \varepsilon_2$ are calculated from finding the eigenvalues of the strain matrix $\begin{pmatrix} \varepsilon_{xx} & \varepsilon_{xy} \\ \varepsilon_{xy} & \varepsilon_{yy} \end{pmatrix}$. Assuming that the volume is constant, the other principal strain is estimated.

$$\varepsilon_3 = -\varepsilon_1 - \varepsilon_2 \tag{8}$$

Finally, the equivalent Von Mises Strain is calculated by

$$\varepsilon_{eq} = \frac{\sqrt{(\varepsilon_1 - \varepsilon_2)^2 + (\varepsilon_1 - \varepsilon_3)^2 + (\varepsilon_3 - \varepsilon_2)^2}}{3} \tag{9}$$

Stochastic Process Modeling

Two-parameter and three-parameter Weibull distributions were used to model stochastic variation of yield strength, ultimate strength, and maximum strain. This modeling in the current effort was based on the guidelines provided in ASTM standards C1683-10(2019), *Standard Practice for Size Scaling of Tensile Strengths Using Weibull Statistics for Advanced Ceramics*, and C1239-13(2018), *Standard Practice for Reporting Uniaxial Strength Data and Estimating Weibull Distribution Parameters for Advanced Ceramics*, performing statistical analysis on material properties of advanced ceramic materials. The equations of two-parameter and three-parameter Weibull distributions are as follows,

$$P(x) = \left(\frac{m}{\beta}\right)\left(\frac{x}{\beta}\right)^{m-1} \exp\left[-\left(\frac{x}{\beta}\right)^{m}\right], x > 0 \tag{10}$$

$$P(x) = \left(\frac{m}{\beta}\right)\left(\frac{x-\theta}{\beta}\right)^{m-1} \exp\left[-\left(\frac{x-\theta}{\beta}\right)^{m}\right], x > 0, \theta > 0 \tag{11}$$

where P is the probability of an event occurring, x is the random variable, m is the Weibull modulus or shape parameter, β is the scale or characteristic value, and θ is the threshold value. Weibull modulus or the shape parameter describes the breadth of the distribution. The higher the value of the Weibull modulus, the lower is the spread of the distribution. The three-parameter Weibull distribution can be used to model data where the possibility of failure under a certain value of the random variable has zero probability. The threshold value is an estimate for the value under which the probability of an event occurring is equal to zero.

Results and Discussion

For the benchmarking studies, commercially sourced stainless steel 304L was used to fabricate the specimens with different coupon geometry and thicknesses. An overlay of engineering stress-strain curves from representative specimens from each category is shown in figure 6. A very close agreement can be seen between the curves up to

FIG. 6

Engineering stress-strain curves obtained from ASTM and MT specimens with a thickness of 0.5 mm, 0.75 mm, and 1 mm.

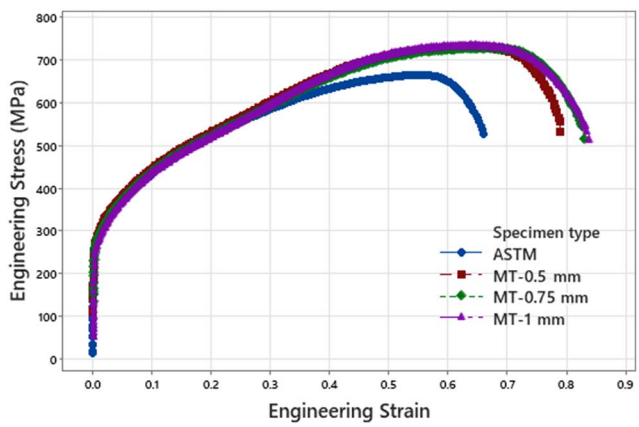

FIG. 7

Fracture surfaces of broken MT specimens.

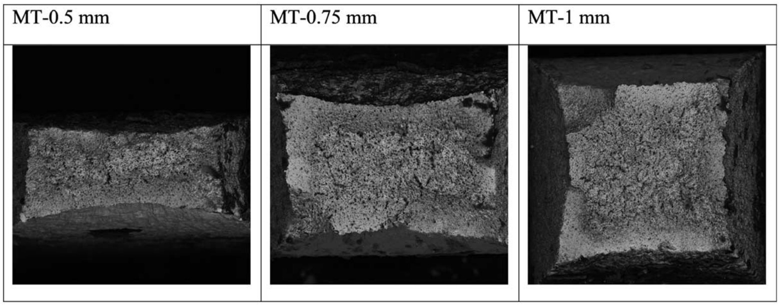

an engineering strain of approximately 30 %. From there on, the strain hardening rate observed from the ASTM specimen was observed to dip and eventually lead to the point of necking and failure. The ultimate strength, strain at ultimate strength which is the measure for uniform deformation, and strain at failure as measured from the ASTM specimen are smaller than those measured from the MT specimens. Among the MT specimens, the specimens with 0.5-mm starting thickness were observed to neck and fail at relatively lower strain at failure. The failure among the MT specimens was observed to be ductile in nature and dimpling or micro-void feature consistent with ductile failure have been observed on the fracture surfaces. The fracture surfaces of representative specimens are shown in figure 7.

To better capture the differences in measurements and realize the scatter in measurements, multiple specimens were tested and compared. The property measurements obtained from engineering strain curves were calculated using the data obtained from an Instron universal testing machine (UTM) and extensometer combination as well as the UTM and the DIC data. The former method was termed conventional, and the latter was termed DIC (see Table 2). As recording the accurate point of strain at break was not reliable using DIC, strain at failure was only obtained using the conventional method. The numbers of specimens tested by specimen design, analysis method, and average and standard deviation values of the measurements are summarized in Table 2.

To compare the statistical significance among differences in property measurements, a one-way analysis of variance and Tukey Means comparison analysis was performed. The strength and ductility measurements from the ASTM measurements were lower than those obtained from the MT specimens. Among the properties, the yield strength measurements from the ASTM specimen were observed to have the least difference when compared to MT counterparts. While statistically significant, the difference in mean values was less than 5 %. On the other hand, the strain at failure was significantly different between the two groups. This is expected and can be attributed to the difference in specimen geometry, aspect ratio, and cross-sectional area.[11]

The UTS measurements were also substantially different. The difference between the ASTM and MT specimens was approximately 10 % of the ASTM values. Two likely reasons were theorized to be the cause of this variation. Firstly, specimen surface finish, and secondly the vastly different defect populations between the gauge volumes. Examining the fracture surfaces of the ASTM specimens, no obvious surface defect-based initiation was observed, and it is therefore unlikely this is the prominent contributing factor. The vastly different defect populations and the differences in the interaction and evolution of the local failures initiating from these defects might explain the variation in ultimate strength values. The likelihood of probabilistic events from different numbers of defects on deformation and failure can be expected to be significantly different between the two gauge volumes.[7,18] To further understand this difference, the equivalent strain field at the point of ultimate strength buildup or the initiation of necking was obtained from DIC analysis. For analyzing this data, histograms to chart the distribution across the gauge length and spatial contour map to realize the location-wise variation was generated (fig. 8). From the contour maps, the local strain was observed to increase in value toward the middle of the gauge length and no

FIG. 8

Histogram of equivalent strain (right column) and spatial variation in equivalent strain in the ASTM and MT specimens at ultimate strength points on the engineering stress-strain curve.

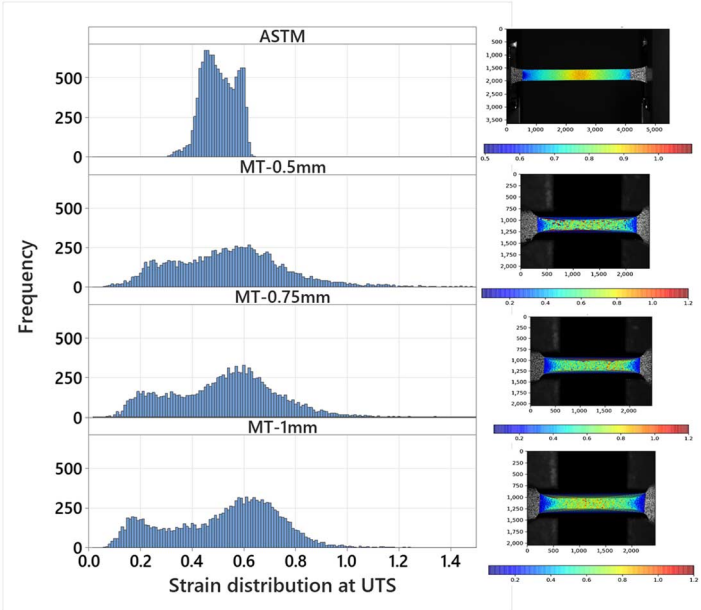

other stress concentration or localization was observed. The spread of local strain values was observed to span vastly different ranges between the ASTM and MT specimen groups. In all the cases, a bimodal distribution of equivalent strain was observed. This may be attributed to strain from uniform deformation and initiation of necking.[18] The mode of the necking strain distribution from the MT specimens was comparable to the peak strain values seen in the ASTM specimens. However, the peak strain values seen in MT specimens were larger than that of the ASTM specimens. Reaching such high values of strain without substantial necking explains the significantly different ultimate strength measurements obtained between the two specimen groups. The MT specimens were able to reach peak local strain values of more than 30-40 % in comparison with the ASTM specimens. This is expected to have facilitated stable strain hardening and therefore higher ultimate strength values. Additionally, among the MT specimens, the peak strain values, and the population levels with strain greater than 0.9 were observed to increase with decreased thickness value. This suggests increasing feasibility for stable deformation and strain with decreasing starting specimen thickness.

To further understand stochastic implications of the gauge volume on property measurements, the property measurements obtained using conventional methods were analyzed. The 0.2 % offset yield strength, UTS, strain at UTS, and strain at break measurements from these specimens were plotted to analyze the scatter and differences among them (see **fig. 9**). Except for the 0.2 % offset yield strength, all the property measurements were found to be a good fit for the three-parameter Weibull distribution. Although a reasonably large group of specimens were tested, the fits were generally difficult to perfectly model the scatter. However, the fits were observed to capture the general trend of variation. A small leftward shift in measurements was observed in the offset yield strength, UTS, and strain at UTS values with decreasing specimen thickness. While the shift was statistically significant, the distributions of these properties were overlapping. The strain at break measurements, however, were found to be significantly different.

From the difference between the strain at break and strain at ultimate strength, the necking strain is a significant contributor to the total strain values. Strain at ultimate strength is not convoluted by the necking strain and can serve as a metric of uniform deformation and ductility. A point to be noted here is that the engineering strain at ultimate strength values are decreasing with thickness, whereas the local strain values seen in **figure 8**

FIG. 9 Weibull fits of conventionally calculated tensile property measurements of MT specimens.

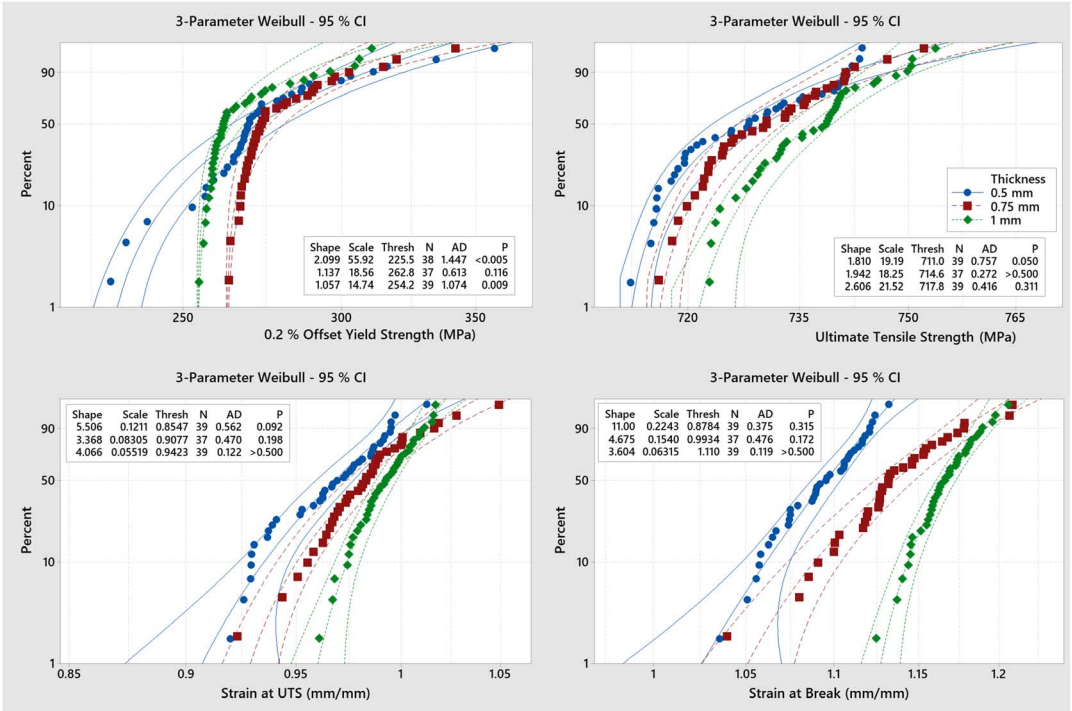

were increasing with decreasing thickness values. This is expected as once local strain peaks, the deformation is localized to these high strain sites during necking, and this can limit any further strain accumulation in the remainder of the gauge section. Accordingly, the strain hardening phenomenon is also capped, and the engineering stress value is capped to the ultimate strength. Therefore, the shift in ultimate strength values also follows the trend of the total strain at ultimate strength and is in reverse of the trend in local peak strain values at ultimate strength.

In summary, this benchmarking study was pursued to catalog the similarities and differences in tensile measurements obtained from the two tensile specimen designs. By doing so, the authors intended to establish the potential for using MT specimens for various characterization and design purposes. Noticeably clear differences in tensile measurements obtained from the MT and ASTM specimens have been documented. There was good agreement between the two specimen stress-strain curves well beyond the yield point. In most cases, the failure criterion for a system is based on the yield phenomenon or a low threshold for plastic deformation. From this study, in the case of AISI 304, it is feasible to utilize MT specimens for material characterization and obtaining basis data for design and other such purposes. Post yield, however, the stress-strain curves tend to diverge between the two specimen designs. This difference is particularly exaggerated in scenarios of large strain values. Applications centered around such large strain and involving small cross-sectional areas would benefit from utilizing the more pertinent MT stress-strain curve data. In applications like mesoscale (or smaller) cellular structures, MT data would be more relevant in providing data needed for design. The need for minimizing over engineering and improvement in prediction accuracy may be addressed by using basis data generated from relevant specimen design on an as-needed basis. In the case of SS304, the strength and ductility values were observed to diminish with increasing gauge volume. This observation is only true for this material and may not necessarily apply to other classes of materials and their alloys. However, the possibility for disagreement between the specimen designs and gauge volumes is clear. The divergence in specimen performance is theorized to be stemming from the vast

differences in defects population and the interaction between competing failure mechanisms during their evolution as the test is progressed. The material tested in the study was fully dense and of good quality. The dominant defect population is expected to be inclusions. Assuming a homogenous dispersion of these defects, fewer inclusions in the smaller MT cross-section could lead to delay in necking initiation and eventual failure. This difference is expected to be substantial with dramatic differences in gauge volume. However, in the case of MT specimens with varying specimen thicknesses, a leftward shift in stochastic performance was captured in the case of ultimate strength and ductility. The authors theorize this is an effect of varying sensitivity/tolerance to a given defect size. For a given defect size, the potential for failure increases with decreasing cross-section size. Based on these differences the authors claim, the MT specimen designs have a high degree of sensitivity to capture stochastic performance variation stemming from the sampling of defect populations in their different conditions.

STRAIN LOCALIZATION IN ADDITIVELY MANUFACTURED POROUS SAMPLES

As evidenced in the preceding section, MT specimen has the potential to stochastically quantify performance variation stemming from defects. In this section, detailed experimentation was conducted to assess the MT specimen's ability to quantify the effect of these defect mechanisms. In the wrought material study, the influence of inclusions on stochastic performance was discussed. To investigate MT specimen's capacity for assessing inhomogeneity (zones including defect mechanisms) within a given material, specimens of porous AISI 304L were assessed. L-PBF, an AM process, was used to intentionally fabricate porous material. The process parameters of the fabrication process were tuned to produce material that was only 97 % dense. The defect structure in the material can be observed from the as-polished and etched images shown in figure 10.

Mini-tensile testing was then employed to identify the influence of porosity on mechanical properties. The strain field at 20 % total elongation and the histogram of the local strain within the region of interest are shown in figure 11. The strain field indicates hot spots where the local strain values are very high. These strain localizations appear to be discrete and spread throughout the gauge length. This is consistent with the porosity that is evenly distributed through the entire volume of the specimen.

From the histogram of local strain values, the spread in the strain is substantial. A bimodal distribution of local strain is observed in the region of interest that was analyzed. The first distribution with a median value of 0.03 approx. is expected to be the region near the fillet on both sides of the gauge length. The second

FIG. 10 Defect structure in the porous AISI 304L fabricated through AM.

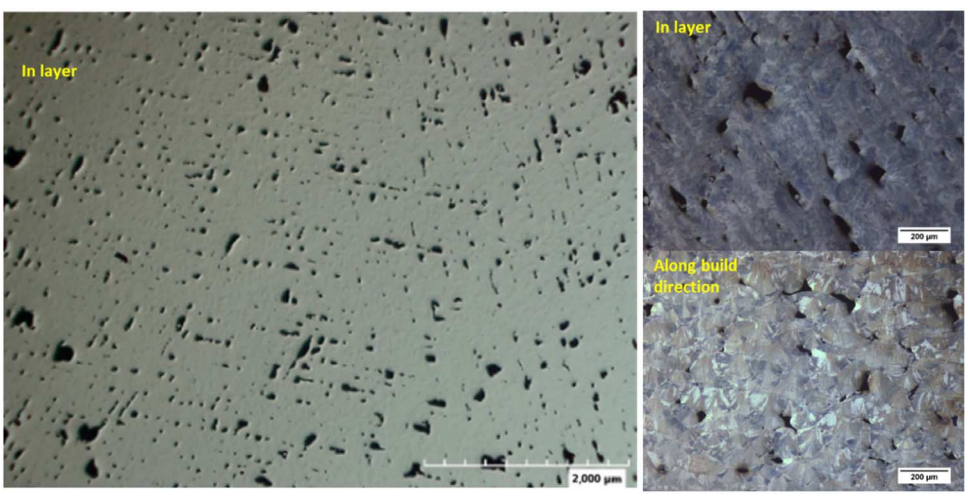

FIG. 11 (*A*) Strain field of a porous specimen at a total elongation of 20 % and (*B*) histogram of local strains from the strain field in (*A*).

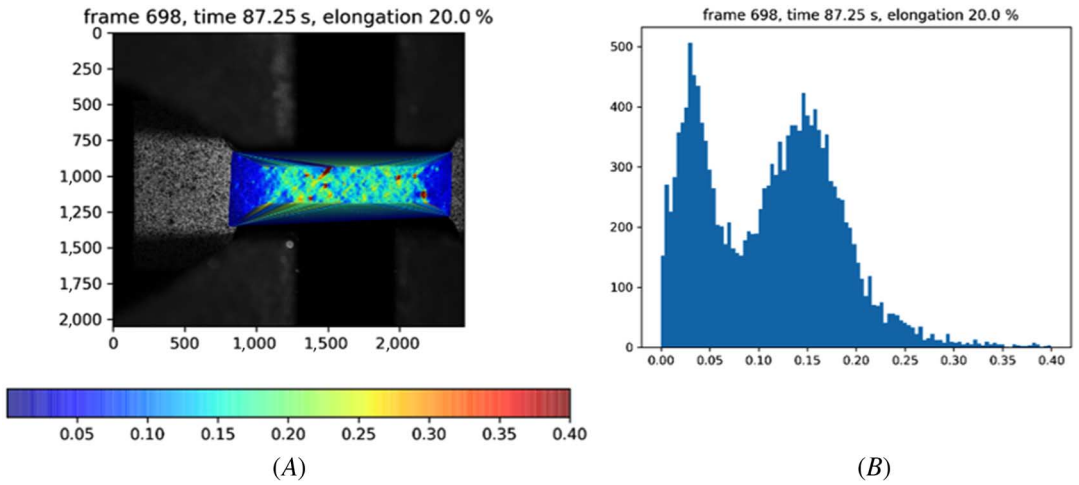

distribution with a median value of approximately 0.16 is expected to be the distribution of the majority of strain across the gauge length. Although the median strain is approximately 0.16, it is significantly less than the total elongation of the specimen. This difference is expected to be compensated by the strain hot spots localized to the locations of porosity.

Whereas the localization of strain was predicted, the development of this localization was visualized using DIC. The set of POIs along the centerline of the gauge length was tracked to realize the strain localization. The local strain value for different total elongation strains is shown in figure 12. As the test progresses, with an increase in total strain, the local strain values were also seen to rise. However, the localization of strain was also seen to rise significantly. The local strain values (spikes in the data) were observed to be as high as two times the value

FIG. 12 (*A*) Values of local strain along the centerline of the gauge length of the porous AISI 304L specimen shown in figure 11 and (*B*) fracture surface of the broken porous mini tensile specimen, the porosity with the material can be seen as pits with spherical powder particles within them.

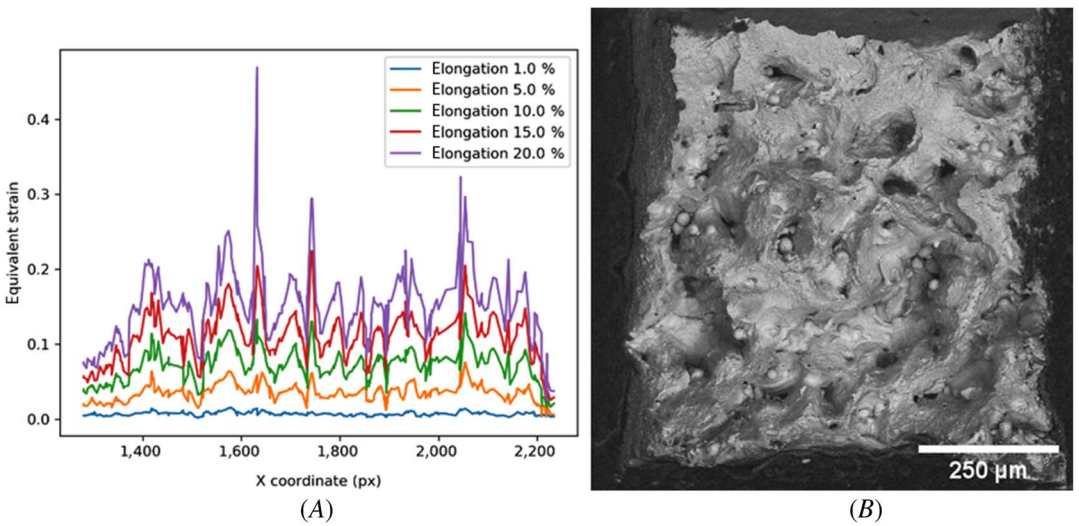

of the total strain. From this, it is clear that the presence of porosity can lead to stress and strain localization. The presence of porosity within the material can also be confirmed from the fracture surface of the broken specimen shown in **figure 12*B***.

To quantify the scatter in the mechanical performance, multiple miniature specimens of the porous 304L stainless steel were prepared and tested. The property measurements were fit to a two-parameter Weibull distribution to model the scatter within the data (see **fig. 13**). The modeling yielded reasonable fits in most cases. The spread in yield and ultimate strength data was very similar. The same was true for the strain at break and strain at ultimate strength values. However, the difference between the strain distributions was not as significant as the difference between the strength values. Upon inspection of the fracture surfaces of the broken specimens, the scatter in the tensile data was attributed to the size of the pores observed on the broken surface. The lower performers had relatively large size pores and surface-connected pores on the fracture surfaces. The presence of porosity is expected to result in a reduction of load-bearing area and ultimately premature failure.

In the previous section, stochastic modeling of MT data from different gauge volume dimensions was theorized to capture the effects of different defect populations. These defect populations could vary in number, size, shape, volume, distribution, etc. Gathering such insights for a defect type such as inclusions can be very time consuming. Therefore, assessing the influence of defect attributes and realizing the sensitivity of MT specimen design for capturing variations in these attributes is also challenging. However, from the study of porous material, the influence of varying porosity is captured in the DIC strain field data and the scatter in tensile properties. The strain localization during the tensile tests and differences in strain among the different strain hot spots can be associated with the differences in defect size. Among these competing hot spots, the weakest "link" is expected to yield faster and become the site of final failure. The variation in the morphology of this weak link is captured in the distribution of the properties seen in stochastic modeling. The porosity seen in this material is expected to span a wide range of sizes while being dispersed uniformly and randomly. Therefore, the scatter captured here could be from weak links with differing morphologies. These differences could be differences in pore size leading

FIG. 13 Two-parameter Weibull fits to model the scatter in the strength and ductility of miniature tensile specimens prepared from porous AISI 304L stainless steel.

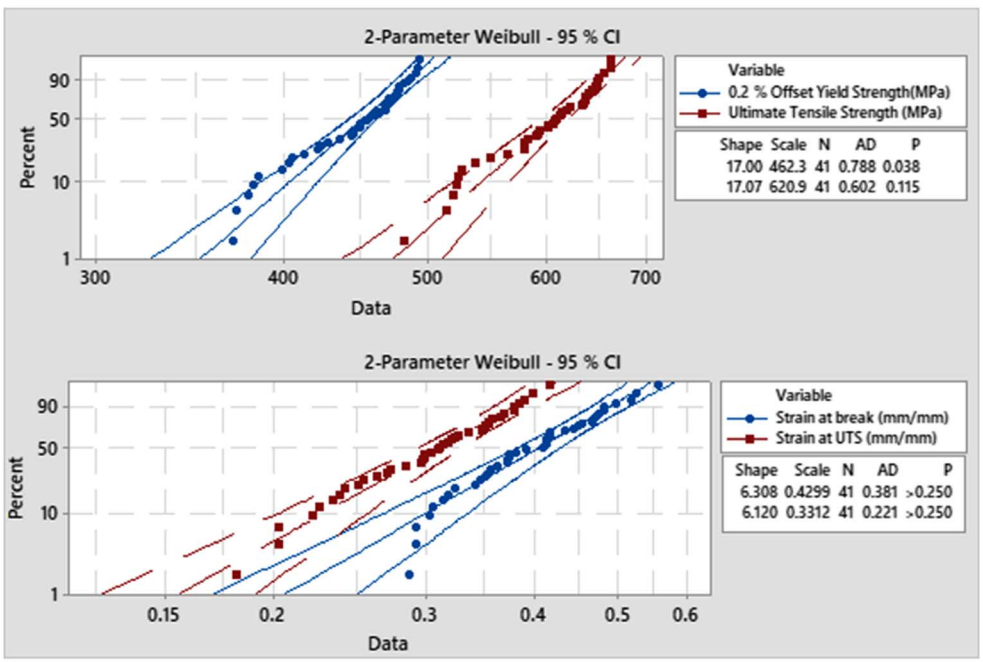

to different load-bearing capacity, coalescence of voids stemming from neighboring porosity, failure initiation from a surface connected open pore, etc. From the stochastics modeling, the MT specimens are theorized to be capable of sampling such variation. Based on these observations, the authors claim MT specimens have high sensitivity for characterizing materials not just in the macroscale but also in the mesoscale as well.

Conclusions

When working with modern materials like FGMs, manufacturing processes like AM, and cellular structural geometries, and other small scale design features in the mesoscale and below, ASTM E8-04 and other standard size specimen testing are less sensitive to capturing the effect of important microstructural features like defects and inclusions on mechanical performance. In this article, the authors proposed an MT specimen design in conjunction with AM made and wrought SS 304L and compared yield strength, UTS between the MT specimen and ASTM E8-04 specimen. Whereas the yield strength data were comparable, the differences observed in the ultimate tensile and the strain at break were statistically significant. For the SS304L used in this study, the strain hardening phenomenon and the effect of defects like inclusions play a significant role in the behavior of material beyond the yield point. Decreasing gauge cross sections and specimen size was theorized to increase the effect that inclusions and defect mechanisms have on mechanical performance, which was observed in this comparative study between the MT and ASTM E8-04 specimen. Understanding these defect mechanisms and the effect they have on mechanical performance is important in the case of materials like FGMs and geometries like cellular structures that are used in a wide range of industries. Therefore, this study was expanded to assess artificially created porosity in AM-made SS 304L. The MT specimen was observed to be sensitive to the presence and morphology of these defect mechanisms, allowing the gathering and analyses of stochastic performance data that indicated the presence of strain hot spots and other microstructural evolution features that statistically affected the performance of the material. Through the evidence presented here, this research team proposes the use of these MT specimen in conjunction with existing ASTM standard testing, especially in cases where the effects of defects and inclusions are critical to the end use application.

ACKNOWLEDGMENTS

SK, SPI, and FL would like to acknowledge the support of the US Department of Energy (Program Manager: Dr. T. Selekler, Award No: DE-SC0018879). We would also like to thank Idaho National Laboratory and Missouri University of Science and Technology for the support provided during this research.

References

1. *Standard Test Methods for Tension Testing of Metallic Materials*, ASTM E8-04 (West Conshohocken, PA: ASTM International, approved April 1, 2004), http://doi.org/10.1520/E8-04
2. K. Kumar, A. Pooleery, K. Madhusoodanan, R. N. Singh, J. K. Chakravartty, B. K. Dutta, and R. K. Sinha, "Use of Miniature Tensile Specimen for Measurement of Mechanical Properties," *Procedia Engineering* 86 (2014): 899–909, https://doi.org/10.1016/j.proeng.2014.11.112
3. A. V. Sergueeva, J. Zhou, B. E. Meacham, and D. J. Branagan, "Gauge Length and Sample Size Effect on Measured Properties during Tensile Testing," *Materials Science and Engineering: A* 526, nos. 1–2 (November 2009): 79–83, https://doi.org/10.1016/j.msea.2009.07.046
4. S. Karnati, I. Axelsen, F. F. Liou, and J. W. Newkirk, "Investigation of Tensile Properties of Bulk and SLM Fabricated 304l Stainless Steel Using Various Gauge Length Specimens" (paper presentation, Solid Freeform Fabrication 2016: Proceedings of the 27th Annual International Solid Freeform Fabrication Symposium—An Additive Manufacturing Conference, Austin, TX, August 8–10, 2016).
5. S. T. Rosinski, A. S. Kumar, S. C. Cannon, and M. L. Hamilton, "Application of Subsize Specimens in Nuclear Plant Life Extension" (paper presentation, ASTM International Symposium on Small Specimen Test Techniques and Their Applications to Nuclear Reactor Vessel Thermal Annealing and Plant Life Extension, New Orleans, LA, January 29–31, 1992).

6. H. Liu, Y. Shen, S. Yang, P. Zheng, and L. Zhang, "A Comprehensive Solution to Miniaturized Tensile Testing: Specimen Geometry Optimization and Extraction of Constitutive Behaviors Using Inverse FEM Procedure," *Fusion Engineering and Design* 121 (October 2017): 188–197, https://doi.org/10.1016/j.fusengdes.2017.07.016
7. V. Karthik, K. Kasiviswanathan, and B. Raj, *Miniaturized Testing of Engineering Materials* (Boca Raton, FL: CRC Press, 2017).
8. S. Miyazaki, K. Shibata, and H. Fujita, "Effect of Specimen Thickness on Mechanical Properties of Polycrystalline Aggregates with Various Grain Sizes," *Acta Metallurgica* 27, no. 5 (May 1979): 855–862, https://doi.org/10.1016/0001-6160(79)90120-2
9. N. Igata, K. Miyahara, T. Uda, and S. Asada, "Effects of Specimen Thickness and Grain Size on the Mechanical Properties of Types 304 and 316 Austenitic Stainless Steel," in *The Use of Small-Scale Specimens for Testing Irradiated Material*, ed. G. E. Lucas (West Conshohocken, PA: ASTM International, 1986), https://doi.org/10.1520/STP33000S
10. Y. Kohno, A. Kohyama, M. L. Hamilton, T. Hirose, Y. Yatoh, and F. A. Garner, "Specimen Size Effects on the Tensile Properties of JPCA and JFMS," *Journal of Nuclear Materials* 283–287, part 2 (December 2000): 1014–1017, https://doi.org/10.1016/S0022-3115(00)00245-2
11. S. Karnati, J. L. Hoerchler, F. Liou, and J. W. Newkirk, "Influence of Gauge Length on Miniature Tensile Characterization of Powder Bed Fabricated 304L Stainless Steel" (paper presentation, Proceedings of the 28th Solid Freeform Fabrication Symposium, Austin, TX, August 7–9, 2017).
12. B. C. Salzbrenner, J. M. Rodelas, J. D. Madison, B. H. Jared, L. P. Swiler, Y. L. Shen, and B. L. Boyce, "High-Throughput Stochastic Tensile Performance of Additively Manufactured Stainless Steel," *Journal of Materials Processing Technology* 241 (October 2016): 1–12.
13. T. Amine, J. W. Newkirk, and R. J. O'Malley, "Evaluating Material Property Variations in Components with Difficult Geometries," in *ASME International Mechanical Engineering Congress and Exposition* (New York: American Society of Mechanical Engineers, 2017).
14. S. Karnati, Y. Zhang, F. F. Liou, and J. W. Newkirk, "On the Feasibility of Tailoring Copper–Nickel Functionally Graded Materials Fabricated through Laser Metal Deposition," *Metals* 9, no. 3 (March 2019): 287, https://doi.org/10.3390/met9030287
15. A. A. Khan, M. B. M. Ali, and N. B. M. Shaffiar, "Relationship of Surface Roughness with Current and Voltage during Wire EDM," *Journal of Applied Sciences* 6, no. 10 (October 2006): 2317–2320, https://orcid.org/10.3923/jas.2006.2317.2320
16. C.-G. Kuo, C.-Y. Hsu, J.-H. Chen, and P.-W. Lee, "Discharge Current Effect on Machining Characteristics and Mechanical Properties of Aluminum Alloy 6061 Workpiece Produced by Electric Discharging Machining Process," *Advances in Mechanical Engineering* 9, no. 11 (November 2017): 1–8, https://doi.org/10.1177/1687814017730756
17. Y. Zhang, S. Karnati, T. Pan, and F. Liou, "Determination of Constitutive Relation from Miniature Tensile Test with Digital Image Correlation," *The Journal of Strain Analysis for Engineering Design* 55, nos. 3–4 (February 2020): 99–108, https://doi.org/10.1177/0309324719892732
18. G. E. Dieter and D. J. Bacon, *Mechanical Metallurgy*, vol. 3 (New York: McGraw Hill, 1976).